Hydrol. Earth Syst. Sci. Discuss., 10, 15295–15335, 2013
www.hydrol-earth-syst-sci-discuss.net/10/15295/2013/
doi:10.5194/hessd-10-15295-2013

Hydrology and Earth System Sciences
Open Access
Discussions

Effects of land-conversion in a biosphere–atmosphere model of Northern South America – Part 1: Regional differences in hydrometeorology

R. G. Knox[1,*], M. Longo[2], A. L. S. Swann[3], K. Zhang[2], N. M. Levine[2], P. R. Moorcroft[2], and R. L. Bras[4]

[1]Massachusetts Institute of Technology, Cambridge, Massachusetts, USA
[2]Harvard University, Cambridge, Massachusetts, USA
[3]University of Washington, Seattle, Washington, USA
[4]Georgia Institute of Technology, Atlanta, Georgia, USA
[*]now at: Lawrence Berkeley National Laboratory, Berkeley, California, USA

Received: 22 October 2013 – Accepted: 6 November 2013 – Published: 13 December 2013

Correspondence to: R. G. Knox (rgknox@lbl.gov)

Published by Copernicus Publications on behalf of the European Geosciences Union.

Abstract

This work investigates how landuse changes over northern South America, driven by human interventions, have affected the regional patterns of hydrology. Comparisons are made to scenarios where no human disturbance of the regional vegetation is assumed. A numerical model of the terrestrial biosphere (Ecosystem Demography Model 2 – ED2) is combined with an atmospheric model (Brazilian Regional Atmospheric Modeling System – BRAMS) to investigate how land conversion in the Amazon and Northern South America have changed the hydrology of the region. Two numerical realizations of the structure and composition of terrestrial vegetation are used as boundary conditions in a simulation of the regional land surface and atmosphere. One realization seeks to capture the present day vegetation condition that includes deforestation and land-conversion, the other is an estimate of the potential structure and composition of the region without human influence. Model output is assessed for consistent and significant pattern differences in hydrometeorology. Results show that South American land conversion has a consistent impact on the regional patterning of precipitation. Land-conversion was not associated with a significant bias in continental mean precipitation, but was associated with a negative bias in mean continental evaporation and a positive bias in continental runoff. A companion paper continues this analysis, with case studies that focus on specific areas that show significant differential hydrologic response.

1 Introduction

The literature documenting land conversion in the Amazon and surrounding areas is significant, the reader is referred to a small selection of non-exhaustive references for some background, (Cardille and Foley, 2003; Skole and Tucker, 1993; INPE, 2003; Nepstad et al., 2001; Geist and Lambin, 2002; Laurance et al., 2001; Nepstad et al., 2001). The seminal studies with General Circulation Models had predicted that massive and widespread Amazonian deforestation would lead to regional reductions in

HESSD
10, 15295–15335, 2013

precipitation, evaporation and moisture convergence, with slight increases in surface temperature (Henderson-Sellers et al., 1993; Nobre et al., 1991; Lean and Warrilow, 1989; Dickinson and Henderson-Sellers, 1988). Higher surface temperatures are thought to be the result of losses in evaporative cooling from the leaf surfaces associated with cleared vegetation. A reduction in atmospheric heating follows a reduction in the heat released by precipitating (condensing) atmospheric water, an assumed consequence of reduced land–atmosphere vapor transport (Eltahir and Bras, 1993). These are two opposing forces to moisture convergence. Positive surface temperature anomalies induce convergent circulations coincident with a decrease in surface pressure. Decreased precipitation heating anomalies reduce tendency towards convergence. While surface temperatures may be higher in deforested areas, there would necessarily be a decrease in total surface energy flux as a direct result of an increased surface albedo (Eltahir, 1996).

The complexity of the Amazonian land–atmosphere feedback system, particularly the nature of secondary feed-backs, supports the need to study this system using more sophisticated numerical modeling with increased granularity. Regional land–atmosphere simulations that can parametrize convective clouds indicate that structured land-conversion scenarios elicit shifts in mean basin precipitation, however less so than traditional coarse scale General Circulation Model studies (Silva et al., 2008). Coherent land surface patterns may strengthen convergence zones on the surface, creating vertical wind triggers to thunderstorms. For instance, Avissar and Werth (2004) introduced that coherent land surface patterns transfer heat, moisture and wave energy to the higher latitudes through thunderstorm activity. Moreover, meso-scale simulations are found to capture key cloud feedback processes which fundamentally alter atmospheric response to land-surface heterogeneities (Medvigy et al., 2011). The meso-scale simulations ability to represent more realistic future land-use scenarios predict an expected redistribution of basin rainfall. For example, western propagating squall-lines from the Atlantic are thought to dissipate over regions of wide-spread deforestation (Silva et al., 2008; d'Almeida et al., 2007). Significant evidence has also shown that convection

HESSD
10, 15295–15335, 2013

can be driven by localized convergent air circulations triggered by land-surface heterogeneities, and that the likelihood and quality of resulting events are both dependent on the scale of heterogeneity and the position relative to disturbed and intact landscapes (Pielke, 2001; Dalu et al., 1996; Baldi et al., 2008; Anthes, 1984; Knox et al., 2011; Wang et al., 2009).

In summary, there has been progress in model based analysis of the land–atmosphere feed-backs resulting from regional land conversion, particularly in the areas of improved granularity and parametrization of physical processes (such as convection). However, the regional ecosystems (the boundary condition governing the different scenarios) in these simulations has yet to be represented with a land surface model that captures the biophysics of forests that feature size, age and composition structure (and the allometric and vertical canopy structure that comes with it). This research investigates the regional scale sensitivities of hydrologic climate in response to present day land conversion in the Amazon and Northern South America. The intent is to continue the collective community modeling effort to increase the physical realism and complexity of the land-surface ecosystems in concert with a meso-scale atmospheric model.

The Ecosystem Demography Model 2 (ED2 or EDM2) (Moorcroft et al., 2001; Medvigy et al., 2009) is coupled with the Brazilian Regional Atmospheric Modeling System (BRAMS). The atmospheric model is a variant of the Regional Atmospheric Modeling System (RAMS) (Cotton et al., 2003), a physical model resolving the three-dimensional fluid momentum equations and a host of physics parametrization tuned for the conditions of the region; turbulent closure, convection, radiative transfer, etc. The Ecosystem-Demography Model 2 is both a dynamic ecosystem model that estimates ecosystem structure and change, as well as a biophysics simulator that conserves the transfer of mass, radiation and enthalpy.

The ED2 model is unique in that it provides a distribution of plant size, plant type and landscape history for every grid-cell that matches the lower boundary of the atmospheric model. The ED2 also provides a representation of the vertical structure and

HESSD
10, 15295–15335, 2013

composition of forest canopies. It accounts for the bio-geochemical fluxes of heat, moisture and carbon through the soil, vegetation and atmosphere. These fluxes modulate the dynamic processes of mortality, reproduction and growth. Its central design philosophy assumes that the stochastic representation of plant communities integrated over a large sample can be portrayed deterministically as land fractions and plant groups, with explicit sizes (of the plants) and age (of the landscape) structure.

This paper will focus on the verification of the experiment design, the process of creating such a detailed realization of the present and potential structures and compositions of the region's ecosystems, and a regional evaluation of the changes in hydrometeorology corresponding to present and potential land-use scenarios. A companion paper, "Part 2: Case study analysis of ecosystem atmospheric interactions", assumes the same experimental methods and model output, and further focuses on case studies within the region to develop a better understanding of the mechanisms associated with land-conversion induced changes to hydrometeorology.

2 Experiment design

The main task of this experiment is to conduct two regional simulations of the South American biosphere and atmosphere. The defining difference between the two simulations is how the biosphere model (ED2) represents the structure (the distribution of plant sizes) and composition (the distribution of plant types) of the region's terrestrial ecosystems, as a consequence of two different disturbance regimes. In one simulation, the vegetation reflects a structure and composition that has no effects of human land-use, i.e., a *Potential Vegetation* (PV) condition. In the other simulation, the model will incorporate an estimate of modern (e.g., 2008) human land-use, i.e., an *Actual Vegetation* (AV) condition. The procedure is broken down into two steps and are elaborated upon; (1) the generation of the *Potential Vegetation* and *Actual Vegetation* structure and composition, and (2) the procedure of simulating the coupled land–atmosphere model that uses the two different vegetation structures as lower boundary conditions.

HESSD
10, 15295–15335, 2013

2.1 Vegetation structure and composition

The creation of the vegetation initial conditions use a "spin-up" process. The spin-up process is an off-line dynamic ED2 simulation, where the driving atmospheric information does not come from a coupled atmospheric model but from a pre-compiled data set derived from the works of Sheffield et al. (2006). The vegetation is initialized with an equal assortment of newly recruited (saplings) plant types. The off-line model is integrated over a period of five hundred years using a best-guess estimate of the historical regional climate.

During spin-up the modeled dynamic vegetation experiences the natural processes of growth, competition, mortality and disturbance. The plant communities evolve to where their distribution of the size and type reaches a quasi equilibrium condition. If ED2 is provided with accurate information regarding plant functional attributes, edaphic condition and climate over a suitably long time, the dynamic vegetation that is simulated will go through a competitive process and emerge to reflect the structure and composition observed in natural landscapes, including demographics of old growth and naturally disturbed forests.

The soil textural information used a combination of databases, this includes (Quesada et al., 2011) within the Amazon basin and a combination of RADAMBRASIL and IGBP-DIS beyond the basin boundaries (Scholes et al., 1995; Rossato, 2001). The climate data used to drive the spin-up process was derived from the UCAR DS314 product (Sheffield et al., 2006)[1]. The DS314 is based on the National Center for Environmental Prediction's Reanalysis Product (NCEP) and maintains the same global and temporal coverage period but has bias corrections and increased resolution based on assimilation of composite data sets. The DS314 surface precipitation record was

[1]Original data sets used in the DS314 are from the Research Data Archive (RDA) which is maintained by the Computational and Information Systems Laboratory (CISL) at the National Center for Atmospheric Research (NCAR). The original Sheffield/DS314 data are available from the RDA (http://dss.ucar.edu) in data set number ds314.0.

HESSD
10, 15295–15335, 2013

further processed such that grid cell average precipitation was downscaled to reflect the point-scale statistical qualities of local rain-gages. This technique used methods of Lammering and Dwyer (2000), and is explained in more detail in Knox (2012). Modified DS314 data from 1970–2005 was repeatedly looped to create a 508 yr climate. A summary of the simulation conditions in the spin-up is covered in Table 1. The ED2 model state of vegetation structure and composition at the end of the multi-century simulation was saved as the *Potential Vegetation* initial condition.

2.2 Actual vegetation boundary condition

The *Actual Vegetation* (AV) was created by continuing the simulation that produced the *Potential Vegetation*, and assumed that the starting year was 1900. This simulation was continued for another 108 yr (until 2008) while incorporating human driven land-use change.

The model applies human land-use by reading in an externally compiled data set of *land-use transition matrices* (Albani et al., 2006). A land-use transition defines the fraction of area of one type of land-cover that will change to another type of land-cover over the course of the year, with units year^{-1}. There are three types of land-cover that transition from one to the other: (1) Primary Forests, (2) Secondary Forests and (3) Converted lands. In model terms, converted lands describe all areas of active human land-use, and are simplified in the model construct as a grassland vegetation structure. Secondary forests are created when pastures are abandoned and when primary forests are degraded by selective logging. Secondary forests can transition to primary forests if they experience natural disturbance (i.e., natural fire or tree-fall).

Two external data sets are used to create the land-use transition matrices, the Global Land-Use data set (GLU) (Hurtt et al., 2006) and the SIMAMAZONIA-1 data set (Soares-Filho et al., 2006). The GLU dataset incorporates the SAGE-HYDE 3.3.1 dataset and provides land-use transitions in its native format globally, on a 1-degree

HESSD
10, 15295–15335, 2013

grid from 1700–1999[2]. The SIMAMAZONIA 1 product provides a more intensive assessment of forest cover and deforestation focused in the Amazon basin, starting in the year 2000. The data is formatted as yearly 1 km forest cover grids (forest, non-forest, natural grasslands), of which yearly transition matrices can be calculated by counting and tallying differences in the classes from year to year.

The transitions from the GLU dataset from 1990–1999 were linearly scaled to have continuity with the SIMAMAZONIA dataset that is introduced in 2000.The transitions from the GLU dataset were gradually scaled from 1976 onward. Note also that the *Actual* ED2 simulation starts in 1900, but prior land-conversion must be accounted for. The land-conversions that occurred before the beginning of the simulation were lumped into a single combined transition applied at the start. A map of the fraction of the land surface containing human land-use is provided (see Fig. 1).

2.3 Above ground biomass – offline model final conditions

regional maps of above ground biomass for the *Potential* vegetation (PV) scenario and the differences between the two scenarios (*Actual*-*Potential*, or AV–PV) are provided in Fig. 2. The majority of above ground biomass in the PV simulation is concentrated in the Amazon basin and the Atlantic Forest of southern Brazil. Late successional broad-leaf evergreens comprise most of the above ground biomass in these regions. Early successional broad-leaf evergreens are a prevalent but secondary contributor to biomass in the Amazon basin. The early successionals contribute the majority of biomass in Cerrado ecotones found roughly in Central Brazil on the southern border of the Amazon rain-forest. This is consistent with their competition and resource niche which emphasizes fast growth and colonization of disturbed areas (such as fire and drought prone Cerrado). Human land-use is concentrated in the Arc of Deforestation,

[2]The use of the SAGE-HYDE 3.3.1 Global Land-use Dataset acknowledges the University of New Hampshire, EOS-WEBSTER Earth Science Information Partner (ESIP) as the data distributor for this dataset.

HESSD
10, 15295–15335, 2013

which is the southern and eastern edge of the Amazon's tropical forests accessible by highways and heavy equipment. Likewise, human land-use has significantly degraded the Atlantic Forest.

The model estimated equilibrium live Above Ground Biomass (AGB) and Basal Area (BA) that represent the initial condition is compared with a collection of census measurements in Baker et al. (2004a, b) (Table 1), see Fig. 3. A map is provided showing the locations of the plot experiments, see Fig. 4. For more detailed information about each census station, please refer to Baker et al. (2004a, b). The coordinates from the measurement stations were matched with ED2 nearest neighbor grid cells. All model cohorts greater than 10 centimeters diameter (DBH) in primary forests were accounted towards the model mean quantities. The published measurements were taken at different times over the previous decades, the lag between these sites and the time of the simulation initial condition (January 2008) varies and is reported. Note that ED2 uses carbon as a prognostic variable during integration. Tree diameter and height is diagnosed from structural carbon, similar to allometric equations in Chave et al. (2001) and Baker et al. (2004b), with differences in parametrization to reflect functional groups. Parameters such as wood density are optimized for plant functional type and modifications are made to allometries when trees reach maximum height before cavitation.

The majority of sites show fair agreement with model estimated above ground biomass and basal area. The exception to this is the cluster of sites located in eastern Bolivia at Huanchaca Dos (HCC), Chore 1 (CHO), Los Fierros Bosque (LFB) and Cerro Pelao (CRP). There are several potential reasons for this discrepancy attributed to the model such as: variability in (1) climate forcing data (most notably precipitation and vapor pressure deficit as these are water limited growth conditions), (2) edaphic conditions and (3) plant functional parameters. These plots are close to the southern Amazonian transition between tropical rain-forests and Cerrado type open canopy forests where gradients in vegetation types are large and uncertainty is expected to be greater. Large spatial gradients in biomass are also reflected in the differences among the cluster of plots (HCC, CHO, LFB and CRP), (124.8 $\mathrm{Mg\,ha^{-1}}$ above ground biomass

HESSD
10, 15295–15335, 2013

at CHO and 260.0 $Mg\,ha^{-1}$ AGB at HCC). The sharp gradient in forest biomass suggests that the omission of sub-pixel variability in the modified DS314 climate forcing could explain a portion of this difference, along with any persistent biases.

2.4 Land–atmosphere coupled simulations

The two coupled land–atmosphere simulations were conducted over four years, 2002–2005. These four years were chosen because of the availability of lateral boundary condition data and validation datasets. With the exception of differing vegetation structure at the lower boundary, the lateral boundary conditions, model parameters, initialization of the atmospheric state, and timing are all identical between the two.

The atmospheric lateral boundary conditions (air temperature, specific humidity, geopotential, meridional wind speed, zonal wind-speed) are taken from the European Centre for Medium Range Weather Forecasting's Interim Reanalysis (ERA-Interim) product (Dee et al., 2011). The data is interpolated from the ERA-Interim's native Reduced Gaussian Grid (N128, which has an equatorial horizontal resolution of 0.75°).

A group of modeling parameters associated with convective parametrization and the radiation scattering of convective clouds were tuned using a manual binary search procedure. The parameters of mean cloud radius, mean cloud depth, cumulus convective trigger mechanism, dynamic control method and the condensate to precipitation conversion efficiency were calibrated against the Tropical Rainfall Measurement Mission 3B43 product and the surface radiation from the Global Energy and Water Cycle Experiment – Surface Radiation Budget product. Fitness metrics include monthly mean spatial bias, mean squared error and the variance ratios. A manual calibration procedure was chosen because of the complexity of the parameter space, the need for human intuition and understanding in connecting parameters to model estimates, and the significant computation requirements for each simulation. Fifty four iterations were performed, utilizing a reduced domain in the first group of iterations to facilitate a more rapid calibration. A table of the finalized coupled model run-time conditions is provided

HESSD
10, 15295–15335, 2013

in Table 2. A comparison of model estimates with observations for mean atmospheric profiles, inter-annual regional precipitation and radiation, and profiles of cloud cover are provided in Appendices A1, A2 and A3 respectively.

3 Comparative analysis of model output

Differences in the patterns of hydrologic output between the coupled model scenarios are presented as differences, calculated by subtracting Potential Vegetation (PV) simulation results from the Actual Vegetation (AV) simulation results. The differential maps (AV–PV) should be interpreted as the net effect of regional land-conversion.

3.1 Emergence of patterning and continental biases

The two simulations show distinct differences in mean annual precipitation patterning, see Fig. 5. There is a persistent dipole pattern of positive differential precipitation in the North and West of the Amazon Delta and negative in the South and East of the Amazon delta region. Another dipole pattern emerges on the Peruvian–Bolivian border, with a positive pole forming to the North of the Andes mountains on the political border extending into northern Bolivia, and the negative pole forming on the southern portion of the border extending into southern Bolivia.

The driving force between the emergence of the dipole precipitation differentials is scrutinized in the companion paper. The analysis focuses on the local patterns of moisture convergence (or divergence) and its relative influence on moist convection compared to the local (surface) generation of instability.

The differential yearly mean down-welling shortwave radiation shows a strong negative correlation with annual precipitation (see Fig. 6). The negative response is strongly influenced by increased cloud optical depth where convective precipitation has increased, and vice-versa. The atmospheric model did not incorporate dynamics of atmospheric gases other than multi-phase water, so changes in optical depth are completely

HESSD
10, 15295–15335, 2013

determined by dynamics in hydrometeors. Maximum mean annual differences in surface irradiance peak at about 10 $W m^{-2}$, and are strongest over the dipole associated with the precipitation differential, as well as over the eastern Brazilian dry lands (41° W).

The differential maps indicate distinct and consistent pattern differences in regional precipitation, but less evidence of an overall continental bias in accumulated precipitation. The mean annual continental bias in accumulated precipitation, evapotranspiration and total runoff is presented in Fig. 7. There was less mean continental precipitation for the Actual Vegetation simulation in 2002, 2004 and 2005. However the difference relative to the total was small, and 2003 does not follow that pattern. A decrease in total continental evapotranspiration and increased runoff associated with human land-conversion was both consistent and more significant from year to year.

Patterns of differential evapotranspiration and transpiration were more strongly pronounced compared with differential precipitation (see Fig. 8). There is a negative bias in both transpiration and total evapotranspiration associated with the "arc of Amazonian deforestation" (starting at 48° W 2° S going clockwise to 62° W 10° S, also see forest biomass differentials in Fig. 2).

3.2 Connections between differential patterns

Deforestation has a direct impact on transpiration by decreasing the stomatal density per unit ground area via the reduction of leaf area index. The reduction in leaf area also directly reduces precipitation interception, with subsequent decreases in leaf surface evaporation and increased through-fall. This combination of factors leads to a distinctly different hydrologic regime, particularly in the arc of deforestation. The increase in precipitation through-fall coupled with the decrease in root water uptake generates a condition of increased runoff (combined surface and sub-surface) and higher equilibrium soil moisture.

These first order effects of deforestation propagate into to secondary effects such as changes in evapotranspiration. The spatial patterns of forest biomass loss (see Fig. 2) and losses in evapotranspiration show modest correlation ($r^2 = 0.4$). The modest

HESSD
10, 15295–15335, 2013

correlation suggests that second order effects and complex system feed-backs account for a significant portion of the variability. These effects include differential precipitation, and potentially the effects of differential surface heating and turbulent transport of scalars (heat and water).

Changes in surface wind-speeds derived from land-conversion induced drag effects could have an influence on the vertical transport of heat and moisture. Maps of the differential in mean wind-speed at 100 m is provided in Fig. 9. Land-conversion is associated with consistent increases in near surface wind-speeds in areas where deforestation is most significant. The effect is most prominent in the most heavily deforested areas of Eastern Para and Rhôndonia Brazil. Note that these areas have particularly high *relative* differences in wind-speed (change per absolute wind-speed). Ubiquitous increases also cover Southern Brazil, Southern Bolivia, Paraguay, Uruguay and Northern Argentina, however the absolute wind-speeds here are relatively large and therefore the relative differences in these areas (particularly northern Argentina and southern Bolivia which are mostly natural grasslands, open forests and cerrado) are not quite as significant as in the heavily deforested areas.

Increases in turbulent transport associated with increased surface wind-speed has the potential to enhance surface heat and energy flux. Firstly, changes in turbulent transport would influence the timing of energy exchange between the surface, which could influence the rates and build-up of surface instability, and potentially shift the Bowen-ratio due to temporal fluctuations in exposed surface water. It is questionable though if mean net surface energy could be changed by increased turbulent transport. Enhanced turbulent transport could drive enhanced sensible surface cooling, resulting in lower equilibrium surface temperature, lower upwelling long-wave radiation, and therefore increased net-radiation and sensible heat flux. This is unlikely the case however, as the differential pattern in sensible heat flux shows no significant spatial correlation with surface wind-speeds, see the lower panels of Fig. 9. Sensible heat fluxes do show modest increases in the dipole where latent heat flux decreased, and vice versa. There is a strong decrease in mean annual sensible heat flux in far eastern

HESSD
10, 15295–15335, 2013

Brazil associated with land-conversion. This was also true for latent heat flux in this region. This is driven by a combination of both increased cloud and surface albedos.

3.3 Significance in hydrologic differentials and ecosystem response

Vegetation response is closely coupled with the availability of photosynthetic active radiation and water. Light and water are critical limiters of plant growth, disturbance (particularly through fire), and mortality (which can be functionally related to growth). The impact that changes in water availability and photosynthetically active radiation have on ecosystem response is dependent on various factors other than differences in the mean, such as the consistency of the differences (inter-annual variance), when the changes occur (seasonality) and how large the differences are relative to the total. A standard score "ζ" provides an metric for consistency. In this case, it is calculated as the inter-annual mean (denoted by brackets "<>") divided by the first standard deviation of the normalized difference η of variable x for year t (mean annual precipitation or down-welling shortwave radiation).

$$\eta_{(t)} = \frac{x_{\mathrm{AV},(t)} - x_{\mathrm{PV},(t)}}{0.5\left(x_{\mathrm{AV},(t)} + x_{\mathrm{PV},(t)}\right)} \quad (1)$$

$$\zeta = \frac{\langle \eta \rangle}{\sigma_{\eta}} \quad (2)$$

The spatial maps of the standard scores are provided in the upper panels of Fig. 10. A standard difference of 1 suggests that the normalized difference is equal to its inter-annual standard deviation. These maps indicate that differential precipitation and radiation are relatively consistent particularly at the dipoles mentioned earlier. It also indicates that the negative precipitation differential, and the positive radiation differential over the regions of intense deforestation (i.e., the Arc of Deforestation) are consistent.

While absolute differences and metrics of consistency identify the significance of differential forcing on ecosystem response, it does not necessarily give an idea if the

HESSD
10, 15295–15335, 2013

vegetation is sensitive to these difference. A metric derived from ED2 model output called the "moisture stress index" msi indicates how susceptible plant communities are to moisture limitation. Each ED2 cohort has an open stomata transpiration rate and a cuticular (closed) stomata transpiration rate. The actual transpiration rate is a linear combination of the open and closed states, weighting the open state by the "stomata open fraction" f'_o. The moisture stress index msi is unity minus the mean stomata open fraction. For an ecosystem with N plant groups (also known as cohorts) indexed i, the mean land-surface moisture stress index is calculated by the leaf area index LAI weighting of the open-fraction f'_o of each plant group in the community. Brackets "<>" denote an averaging in space and time.

$$\text{msi} = 1 - \left\langle \frac{\sum_{i=1}^{N} \text{LAI}_{(i)} f'_{o(i)}}{\sum_{i=1}^{N} \text{LAI}_{(i)}} \right\rangle \tag{3}$$

The ED2 model uses the stress function to scale the fraction of time a plant has stomata in the open or closed state. It calculates f'_o based on the ratio of the plant's demand for root zone soil moisture, and the supply of water the roots are capable of extracting at that time. The demand requirement is driven by the maximum potential transpiration the plant would generate given the light, carbon and vapor pressure conditions with unlimited soil moisture.

$$f'_{o(i)} = \frac{1}{1 + \frac{\text{Demand}}{\text{Supply}}} \tag{4}$$

The structure and composition of ecosystems that have high moisture stress indices are more likely to respond to significant changes in precipitation. The panels of Fig. 10 provide a more comprehensive assessment of the the significance of differential precipitation and radiation, as well as ecosystem susceptibility to change. Note that the interior of the Amazon basin has little to no influence of moisture stress on photosynthesis and growth.

HESSD
10, 15295–15335, 2013

Two locations that coincide with the dipole precipitation lobes are highlighted in Fig. 10. Each location shows significant and consistent decreases in precipitation and increases in down-welling short-wave radiation associated with the *Actual Vegetation* case. The vegetation of these locations also show varying degrees of moisture stress. The differential surface hydrology and hydrometeorology of these locations will be explored in more detail in the companion paper, "Part II: Case study analysis of ecosystem atmospheric interactions".

4 Conclusions

The simulation results have shown that land conversion, as it defines the regional structure of vegetation in 2008, has influenced the patterning of South American precipitation. In two locations a dipole phenomenon emerges in the differential precipitation, one near Eastern Para and one near the Peru–Bolivia border. An assessment of regional moisture stress indices (msi) indicate that terrestrial vegetation in these two regions show moderate to significant susceptibility to changes in water availability (precipitation). Precipitation differentials have shown inter-annual consistency, and as will be covered in greater detail during the companion paper, are expressed mostly in the late dry-season (Para in September) and the early dry season (Bolivia in April).

Results indicate that land conversion in South America has not had a significant influence on continental mean precipitation. Continental mean precipitation with land conversion decreased in three out of four simulation years, but the differences were insignificant. On the other hand, differences in mean continental runoff (increased with land-conversion scenario) and total evapotranspiration (decreased with land-conversion scenario) were consistent and significant from year to year.

Spatial maps the differentials in first order hydrologic responses showed moderate correlations with spatial patterns of differential biomass, i.e., decreases in evapotranspiration accompanied decreases in biomass due to land-conversion. This is attributed to two mechanisms. Firstly, land conversion in forested regions decreases leaf

HESSD
10, 15295–15335, 2013

interception of precipitation. Precipitation that is intercepted by the canopy is more likely to be re-evaporated to the atmosphere, as precipitation through-fall has a relatively greater likelihood (compared to leaf intercepted water) to exit the land-surface as runoff. Secondly, conversion of forested lands directly reduces transpiration. The total transpiration of a landscape is strongly influenced by the the stomatal density and leaf area, both of which are reduced with land-conversion and deforestation.

It is noteworthy that the decrease in differential transpiration (and root-zone uptake) and increased differential through-fall fraction mediates increased runoff at least partially through an increase in equilibrium total column soil moisture. This research highlighted the use of a relatively advanced ecosystem model that features a vertically structured canopy and soil moisture layering system and improved realism in the regional distribution of above ground biomass. Further studies that incorporate these improvements in vertical structure and regional biomass, with modules that advance and capture the horizontal transport of surface and sub-surface moisture could improve our understanding of how deforestation impacts runoff and how differential runoff may feedback on ecosystem function and land–atmosphere interaction. This work does make the case, at the continental scale and particularly in areas of significant deforestation, that land-conversion has significantly altered the partitioning of hydrologic flux at the land-surface in Northern South America.

Appendix A

Comparison of ED2-BRAMS model output with observations

A1 Thermodynamic mean profiles

The objectives of this experiment require that modeling system output match mean observations to such a degree that there is trust in the model's ability to represent physical processes. It is believed that the relative differences between the two simulations have

HESSD
10, 15295–15335, 2013

validity if model processes reproduce mean observed tendencies in the land surface and atmosphere.

Mean monthly profiles of model estimated air temperature, specific humidity and moist static energy are compared with mean radiosonde data over Manaus Brazil (see Figs. 11 and 12). Comparisons are made at 00:00 and 12:00 UTC. The model estimates a consistently warmer atmosphere, in the range of about two degrees both morning and evening. Model estimated specific humidity in the lower troposphere is lower than the radiosondes (see Fig. 11). Moist static energy is slightly underestimated by the model in the lower troposphere and then overestimated in the mid to upper troposphere. This may suggest that the model is convecting relatively large quantities of warm moist air at the surface and entraining it to the upper atmosphere.

A2 Inter-seasonal precipitation and surface radiation

Monthly precipitation and down-welling shortwave radiation in the model is evaluated as spatial means within five separate zones of analysis. The boundaries of the zones of analysis are shown in Fig. 4. Monthly mean model estimates are again compared to precipitation estimates from the Tropical Rainfall Measurement Mission 3B43 product and surface radiation from the GEWEX Surface Radiation Budget product. There is generally acceptable agreement between the model and TRMM estimated precipitation. The seasonal variability in both datasets is greater than their differences (see Fig. 13). The most significant differences are the strength of of the wet-season peak precipitation in Zone 3 (central-eastern Amazon) and the severity of the dry season precipitation in Zone 5 (Southern Brazil). The timing of peak and minimum rainfall show generally good agreement, particularly in Zones 2–5. The lower estimate of mean precipitation in Southern Brazil is consistent with decreased cloud albedo and increased down-welling short-wave radiation at the surface (see Fig. 14). Surface shortwave radiation has a modest under-estimating bias compared with the SRB estimates for most other cases.

HESSD
10, 15295–15335, 2013

A3 All-sky cloud water content profiles

Cloud profile validation datasets were constructed from CloudSat Cloud Water content (2B-CWC-RO) and Cloud Classification (2B-CLDCLASS-LIDAR) datasets.[3] Overpasses during February 2007–2011 that intersected the geographic subset between 3° N–12° S and 70–55° W were collected and interpolated to a constant vertical datum above the surface. Overpasses typically occurred near 17:00 UTC.

The comparison was not expected to be that good. The simulation time frame does not overlap with the CloudSat mission time-frame. CloudSat measurements are known to have signal loss, attenuation and clutter during moderate to intense rainfall; events such as these could not be filtered from the comparison. It must also be assumed that the cloud classification algorithm is not without error. Nonetheless, the purpose of the comparison was to get a sense of whether the simulations estimated reasonable mean ranges of water contents and cloud fractions, and also if the phase transitions (liquid to ice) were occurring at reasonable elevations.

The all-sky cloud water content profiles for both cumulus and non-cumulus clouds are provided in Fig. 15. The peaks in model estimated mean cloud water content showed reasonable agreement across liquid and ice cloud types. The model estimated generally more water content in both phases, skewed towards higher altitudes and showed a uni-modal shape in the vertical distribution. It is possible that CloudSat relative underestimation could be explained by the omission of precipitating clouds.

Acknowledgements. This work was made possible through both the National Science Foundation Grant ATM-0449793 and National Aeronautics and Space Administration Grant NNG06GD63G. The authors would like to thank D. Entekhabi and E. A. B. Eltahir for their generous discussion and council.

[3]Cloudsat datasets were provided on-line by CloudSat Data Processing Center, courtesy of NASA, Colorado State University and their partners.

HESSD
10, 15295–15335, 2013

References

Albani, M., Medvigy, D., Hurtt, G. C., and Moorcroft, P. R.: The contributions of land-use change, CO_2 fertilization, and climate variability to the Eastern US carbon sink, Global Change Biol., 12, 2370–2390, 2006. 15301

Anthes, R. A.: Enhancement of convective precipitation by mesoscale variations in vegetative covering in semiarid regions, J. Clim. Appl. Meteorol., 23, 541–554, 1984. 15298

Baker, T., Phillips, O., Malhi, Y., Almeida, S., Arroyo, L., Fiore, A. D., Erwin, T., amd T. J. Killeen, N. H., Laurance, S., Laurance, W., Lewis, S., Monteagudo, A., Neill, D., Vargas, P., Pitman, N., Silva, N., and Vasquez-Martinez, R.: Increasing biomass in Amazonian forest plots, Philos. T. Roy. Soc. B, 359, 353–365, 2004a. 15303, 15323, 15324

Baker, T., Phillips, O., Malhi, Y., Almeida, S., Arroyo, L., Fiore, A. D., Erwin, T., Killeen, S., Laurance, S., Laurance, W., Lewis, S., Lloyd, J., Monteagudo, A., Neill, D., Patino, S., Pitman, N., Silva, N., and Martinez, R. V.: Variation in wood density determines spatial patterns in Amazonian forest biomass, Global Change Biol., 10, 545–562, 2004b. 15303, 15319, 15323, 15324

Baldi, M., Dalu, G. A., and Pielke, R. A.: Vertical velocities and available potential energy generated by landscape variability – theory, J. Appl. Meteorol. Clim., 47, 397–410, 2008. 15298

Beljaars, A. C. M. and Holtslag, A. A. M.: Flux parameterization over land surfaces for atmospheric models, J. Appl. Meteorol., 30, 327–341, 1991. 15319

Cardille, J. and Foley, J.: Agricultural land-use change in Brazilian Amazonia between 1980 and 1995: evidence from integrated satellite and census data, Remote Sens. Environ., 87, 551–562, 2003. 15296

Chave, J., Riera, B., and Dubois, M.: Estimation of biomass in a neotropical forest of French Guiana: spatial and temporal variability, J. Trop. Ecol., 17, 79–96, 2001. 15303, 15319

Chen, C. and Cotton, W.: A one-dimensional simulations of the stratocumulus-capped mixed layer, Bound.-Lay. Meteorol., 25, 289–321, 1983. 15320

Collatz, G. J., Ball, J., Grivet, C., and Berry, J. A.: Physiological and environmental regulation of stomatal conductance, photosynthesis and transpiration: a model that includes a laminar boundary layer, Agr. Forest. Meteorol., 54, 107–136, 1991. 15319

Collatz, G. J., Ribas-Carbo, M., and Berry, J.: Coupled photosynthesis-stomatal conductance model for leaves of C_4 plants, Aust. J. Plant Physiol., 19, 519–538, 1992. 15319

HESSD
10, 15295–15335, 2013

Cotton, W., Pielke, R., Walko, R., Liston, G., Tremback, C., Jiang, H., McAnelly, R., Harrington, J., Nicholls, M., Carrio, G., and McFadden, J.: RAMS 2001: current status and future directions, Meteorol. Atmos. Phys., 82, 5–29, 2003. 15298

d'Almeida, C., Vörösmarty, C. J., Hurtt, G. C., Marengo, J. A., Dingman, S. L., and Keim, B. D.: The effects of deforestation on the hydrological cycle in Amazonia: a review on scale and resolution, Intl. J. Climatol., 27, 633–647, 2007. 15297

Dalu, G. A., Pielke, R. A., Baldi, M., and Zeng, X.: Heat and momentum fluxes induced by thermal inhomogeneities, J. Atmos. Sci., 53, 3286–3302, 1996. 15298

Dee, D. P., Uppala, S. M. Simmons, A. J. Berrisford, P., Poli, P., Kobayashi, S., Andrae, U., Balmaseda, M. A., Balsamo, G., Bauer, P., Bechtold, P., Beljaars, A. C. M., van de Berg, L., Bidlot, J., Bormann, N., Delsol, C., Dragani, R., Fuentes, M., Geer, A. J., Haimberger, L., Healy, S. B., Hersbach, H., Hólm, E. V., Isaksen, L., Køllberg, P., Köhler, M., Matricardi, M., McNally, A. P., Monge-Sanz, B. M., Morcrette, J. J., Park, B. K., Peubey, C., de Rosnay, P., Tavolato, C., Thépaut, J. N., and Vitart, F.: The ERA-Interim reanlysis: configuration and performance of the data assimilation system, Q. J. Roy. Meteorol. Soc., 137, 553–597, 2011. 15304

Dickinson, R. and Henderson-Sellers, A.: Modeling tropical deforestation: a study of GCM land-surface parameterizations, Q. J. Roy. Meteorol. Soc., 114, 439–462, doi:10.1002/qj.49711448009, 1988. 15297

Dietze, M., Wolosin, M., and Clark, J.: Capturing diversity and inerspecific variability in allometries: a hierarchical approach, Forest Ecol. Manage., 256, 1939–1948, 2008. 15319

Eltahir, E. and Bras, R.: On the response of the tropical atmosphere to large-scale deforestation, Q. J. Roy. Meteorol. Soc., 119, 779–793, 1993. 15297

Eltahir, E. A. B.: Role of vegetation in sustaining large-scale atmospheric circulations in the tropics, J. Geophys. Res.-Atmos., 101, 4255–4268, doi:10.1029/95JD03632,1996. 15297

Freitas, S. R., Rodrigues, L. F., Longo, K. M., and Panetta, J.: Impact of a monotonic advection scheme with low numerical diffusion on transport modeling of emissions from biomass burning, J. Adv. Model. Earth Syst., 4, 1–26, doi:10.1029/2011MS000084, 2012. 15320

Geist, H. and Lambin, E.: Proximate causes of underlying driving forces of tropical deforestation, Bioscience, 52, 143–150, doi:10.1641/0006-3568(2002)052[0143:PCAUDF]2.0.CO;2, 2002. 15296

HESSD
10, 15295–15335, 2013

Grell, G. A. and Dévényi, D.: A generalized approach to parameterizing convection combining ensemble and data assimilation techniques, Geophys. Res. Lett., 29, 38-1–38-4, doi:10.1029/2002GL015311, 2002. 15320

Harrington, J. and Olsson, P.: A method for the parameterization of cloud optical properties in bulk and bin microphysical models, implications for arctic cloud boundary layers, Atmos. Res., 57, 51–80, 2001. 15320

Henderson-Sellers, A., Dickinson, R., Durbridge, T., Kennedy, P., McGufie, K., and Pitman, A.: Tropical deforestation: modeling local to regional scale climate change, J. Geophys. Res., 98, 7289–7315, 1993. 15297

Hurtt, G. C., Frolking, S., Fearon, M. G., Moore, B., Shevialokova, E., Malyshev, S., Pacala, S. W., and Houghton, R. A.: The underpinnings of land-use history: three centuries of global gridded land-use transitions, wood harvest activity and resulting secondary lands, Global Change Biol., 12, 1–22, 2006. 15301

INPE: Monitoring of the Amazon forest by satellite 2001–2002, Instituto Nacional de Pesquisas Espaciais, Technical Paper, Sao Jose Dos Campos, Brazil, 2003. 15296

Kain, J.: The Kain-Fritsch convective parameterization: an update, J. Appl. Meteorol., 43, 170–181, 2004. 15320

Kain, J. and Fritsch, J.: A one-dimensional entraining-detraining plume model and its application in convective parameterization, J. Atmos. Sci., 47, 2784–2802, 1990. 15320

Knox, R.: Land Conversion in Amazonia and Northern South America; Influences on Regional Hydrology and Ecosystem Response, Ph. D. thesis, Massachusetts Institute of Technology, Cambridge, Massachusetts, USA, 2012. 15301

Knox, R., Bisht, G., Wang, J., and Bras, R.: Precipitation variability over the forest-to-nonforest transition in southwestern Amazonia, J. Climate, 24, 2368–2377, 2011. 15298

Lammering, B. and Dwyer, I.: Improvement of water balance in land surface schemes by random cascade disaggregation of rainfall, Int. J. Climatol., 20, 681–695, 2000. 15301

Laurance, W., Cochrane, M., Bergen, S., Fearnside, P., Delamonica, P., Barber, C., D'Angelo, S., and Fernandes, T.: The future of the Brazilian Amazon, Science, 291, 438–439, doi:10.1126/science.291.5503.438, 2001. 15296

Lean, J. and Warrilow, D.: Simulation of the regional climatic impact of amazon deforestation, Nature, 342, 411–413, 1989. 15297

Leuning, R.: A critical appraisal of a combined stomatal-photosynthesis model for C_3 plants, Plant Cell Environ., 18, 339–355, 1995. 15319

HESSD
10, 15295–15335, 2013

Massman, W.: An analytical one-dimensional model of momentum transfer by vegetation of arbitrary structure, Bound.-Lay. Meteorol., 83, 407–421, 1997. 15319
Medvigy, D., Wofsy, S., Munger, J., Hollinger, D., and Moorcroft, P.: Mechanistic scaling of ecosystem function and dynamics in space and time: ecosystem demography model version 2, J. Geophys. Res., 114, 1–21, 2009. 15298, 15319
Medvigy, D., Walko, R., Otte, M., and Avissar, R.: The ocean–land–atmosphere-model: optimization and evaluation of simulated radiative fluxes and precipitation, Mon. Weather Rev., 138, 1923–1939, 2010. 15320
Medvigy, D., Walko, R., and Avissar, R.: Effects of deforestation on spatiotemporal distributions of precipitation in South America, J. Climate, 24, 2147–2163, 2011. 15297
Moorcroft, P., Hurtt, G., and Pacala, S.: A method for scaling vegetation dynamics: the ecosystem demography model, Ecol. Monogr., 71, 557–586, 2001. 15298
Nakanishi, M. and Niino, H.: An improved Mellor-Yamada level-3 model with condensation physics: its numerical stability and application to a regional prediction of advection fog, Bound.-Lay. Meteorol., 119, 397–407, 2006. 15320
Nepstad, D., Carvalho, G., Barros, A., Alencar, A., Capobianco, J., amd P. Moutinho, J. B., Lefebvre, P., Silva, U. L., and Prins, E.: Road paving, fire regime feedbacks and the future of amazon forests, Forest Ecol. Manage., 154, 395–407, 2001. 15296
Nobre, C., Sellers, P., and Shukla, J.: Amazonian deforestation and regional climate change, J. Climate, 4, 957–988, doi:10.1175/1520-0442(1991)004<0957:ADARCC>2.0.CO;2, 1991. 15297
Pielke, R.: Influence of the spatial distribution of vegetation and soils on the prediction of cumulus convective rainfall, Rev. Geophys., 39, 151–171, 2001. 15298
Poorter, L., Bongers, L., and Bongers, F.: Architecture of 54 moist-forest tree species: traits, trade-offs and functional groups, Ecology, 87, 1289–1301, 2006. 15319
Quesada, C. A., Lloyd, J., Anderson, L. O., Fyllas, N. M., Schwarz, M., and Czimczik, C. I.: Soils of Amazonia with particular reference to the RAINFOR sites, Biogeosciences, 8, 1415–1440, doi:10.5194/bg-8-1415-2011, 2011. 15300, 15319
Rossato, L.: Estimativa da capacidade de armazenamento de água no solo do Brasil, Msc. thesis, Instituto Nacional de Pesquisas Espaciais (INPE), São José dos Campos, Brazil, 2001. 15300

HESSD
10, 15295–15335, 2013

Scholes, R., Skole, D., and Ingram, J. S. (Eds.): A Global Database of Soil Properties: Proposal for Implementation, Report of the Global Soils Task Group, Tech. Rep. IGBP-DIS Working Paper 10a, International Geosphere-Biosphere Programme – Data and Information System (IGBP-DIS), University of Paris, Paris, France, 1995. 15300

Sheffield, J., Goteti, G., and Wood, E.: Development of a 50-Year high-resolution global dataset of meteorological forcings for land surface modeling, J. Climate, 19, 3088–3111, 2006. 15300, 15319

Silva, R. R. D., Werth, D., and Avissar, R.: Regional impacts of future land-cover changes on the Amazon basin wet-season climate, J. Climate, 21, 1153–1170, 2008. 15297

Skole, D. and Tucker, C.: Tropical deforestation and habitat fragmentation in the Amazon: satellite data from 1978 to 1988, Science, 260, 1905–1910, 1993. 15296

Soares-Filho, B. S., Nepstad, D., Curran, L. M., Cerqueira, G. C., Garcia, R., Ramos, C. A., Voll, E., McDonald, A., Lefebvre, P., and Schlesinger, P.: Modelling conservation in the Amazon basin, Nature, 440, 520–523, doi:10.1038/nature04389, 2006. 15301

Tremback, C. and Kessler, R.: A surface temperature and moisture parameterization for use in mesoscale models, Preprints, Seventh Conf. on Numerical Weather Prediction, Montreal, PQ, Canada, Amer. Meteor. Soc., 355–358, 1985. 15319

Walcek, C. and Aleksic, N.: A simple but accurate mass conservative, peak-preserving, mixing ratio bounded advection algorithm with Fortran code, Atmos. Environ., 32, 3863–3880, 1998. 15320

Walko, R., Band, L., Baron, J., Kittel, T., Lammers, R., Lee, T., Ojima, D., Pielke, R., Taylor, C., Tague, C., Tremback, C., and Vidale, P.: Coupled atmosphere-biophysics-hydrology models for environmental modeling, J. Appl. Meteorol., 39, 931–944, 2000. 15319

Wang, J., Chagnon, F., Williams, E., Betts, A., Renno, N., Machado, L., Bisht, G., Knox, R., and Bras, R.: The impact of deforestation in the Amazon basin on cloud climatology, P. Natl. Acad. Sci. USA, 106, 3670–3674, 2009. 15298

Zhao, W. and Qualls, R. J.: A multiple-layer canopy scattering model to simulate shortwave radiation distribution within a homogeneous plant canopy, Water Resour. Res., 41, W08409, doi:10.1029/2005WR004016, 2005. 15319

Zhao, W. and Qualls, R. J.: Modeling of long-wave and net radiation energy distribution within a homogeneous plant canopy via multiple scattering processes, Water Resour. Res., 42, W08436, doi:10.1029/2005WR004016, 2006. 15319

HESSD
10, 15295–15335, 2013

Table 1. Simulation constraints describing the spin-up process creating the initial boundary conditions.

Specification	Value
climate data	modified DS314*
soils data	Quesada et al. (2011) + IGBP-DIS
plant types	late succession tropical evergreens
	mid succession tropical evergreens
	early succession tropical evergreens
	subtropical grasses
	C4 grasses
simulation period	508 yr
spatial resolution	gridded 1°
bounding domain	30° S–15° N, 85–30° W
tree allometry	
(DBH, height)	Chave et al. (2001); Baker et al. (2004b)
(crown properties)	Poorter et al. (2006); Dietze et al. (2008)
turbulent transport	Beljaars and Holtslag (1991) atmospheric boundary
	Massman (1997) within canopy
photosynthesis	Collatz et al. (1991)
and leaf conductance	Collatz et al. (1992)
	Leuning (1995)
canopy radiation scattering	Zhao and Qualls (2005, 2006)
soil hydrology	Walko et al. (2000); Tremback and Kessler (1985)
	Medvigy et al. (2009)

* Modified DS314 data is derived from Sheffield et al. (2006), precipitation downscaling and radiation interpolation is applied, see footnote for data availability.

HESSD
10, 15295–15335, 2013

Table 2. Run time parameters and specifications in the ED2-BRAMS coupled simulations.

Specification	Value
grid projection	polar stereographic
grid dimensions	98 (E–W), 86 (N–S), 56 (vertical)
horizontal grid resolution	64 km
vertical grid resolution	110 m (lowest) stretching to 1500 m at 7 %
method of calculating	level of maximum sum of mean
updraft base	and variance of vertical velocity
number of prototype cloud scales	2
mean radius of cloud 1	20 000 m
minimum depth of cloud 1	4000 m
mean radius of cloud 2	800 m
minimum depth of cloud 2	80 m
cumulus convective scheme	Grell and Dévényi (2002)
cumulus convective trigger	pressure differential between updraft base and LFC* < 100 hpa
cumulus dynamic control	Kain and Fritsch (1990); Kain (2004)
condensate to precipitation conversion efficiency	3 %
cloud #concentrations and distribution parameters	Medvigy et al. (2010)
turbulent closure	Nakanishi and Niino (2006)
short-wave radiation scattering	Harrington and Olsson (2001)
long-wave radiation scattering	Chen and Cotton (1983)
advection	monotonic, Walcek and Aleksic (1998) and Freitas et al. (2012)
cumulus feedback on radiation?	Yes

[a] LFC = Level of Free Convection.

HESSD
10, 15295–15335, 2013

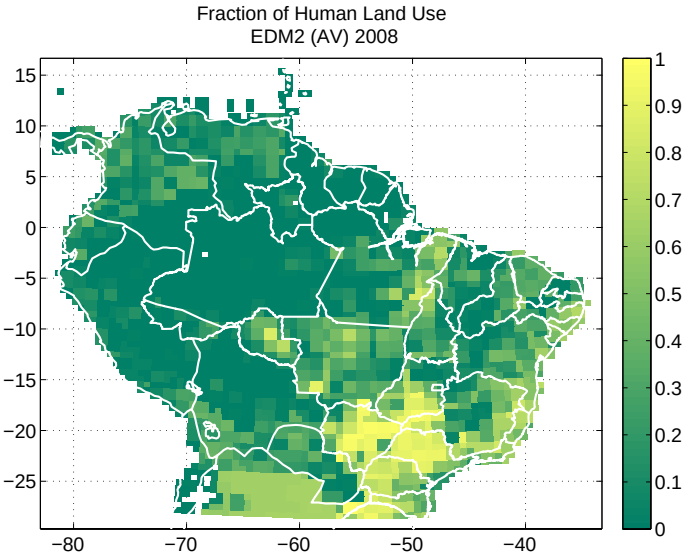

Fig. 1. Fraction of the land surface with human land-use, as described by ED2 the *Actual Vegetation* (AV) simulation result.

HESSD
10, 15295–15335, 2013

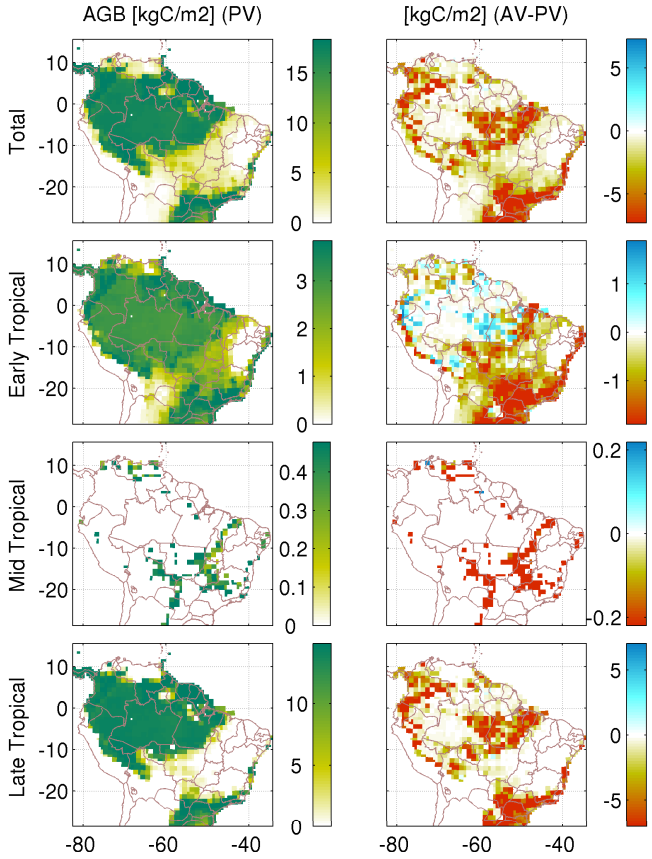

Fig. 2. Regional maps of total Above Ground Biomass (AGB) [kg m^{-2}] from the ED2 initial condition. AV: Actual Vegetation and PV: Potential Vegetation conditions. The left column indicates results are from the Potential Vegetation condition, the right column is the relative difference ($AGB_{AV} - AGB_{PV}$). The above ground biomass is also partitioned by relevant woody plant functional groups.

HESSD
10, 15295–15335, 2013

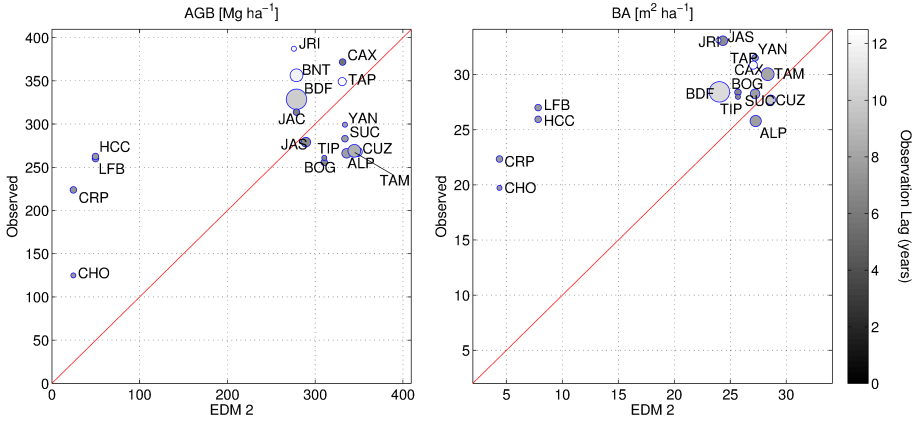

Fig. 3. Comparison of model estimated mean Above Ground Biomass (AGB) and Basal Area (BA) with measurements presented in Baker et al. (2004a, b) Circle size shows relative approximation of the number of census sites used in the field measurements reported in Baker (maximum = 11 separate plots at BDF). Darker circles indicate that measurements were taken more recently and therefore have less time-lag in the comparison with the ED2 initial condition (January 2008). In accord with methods of Baker et al. (2004a, b), model estimates were filtered to include only primary forests and ignored vegetation less than 10 cm diameter. Coarse woody debris was excluded from comparison, only live stems were accounted for.

HESSD
10, 15295–15335, 2013

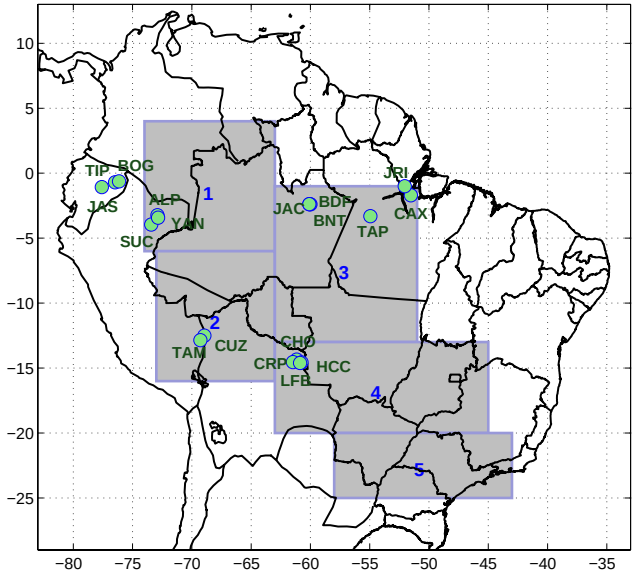

Fig. 4. Locations of zones and sites of analysis. Zones are numbered 1 through 5, and reflect geographic areas where model and observation spatial means are compared for validation (see Appendix). Forest census plot sites from Baker et al. (2004a, b) are referenced with green markers and their station code. Station codes designate the following site names: Allpahuayo (ALP), BDFFP (BDF), Bionte (BNT), Bogi (BOG), Caxiuana (CAX), Chore (CHO), Cerro Pelao (CRP), Cuzco Amazonico (CUZ), Huanchaca Dos (HCC), Jacaranda (JAC), Jatun Sacha (JAS), Jari (JRI), Los Fierros Bosque (LFB), Sucusari (SUC), Tambopata (TAM), Tapajos (TAP), Tiputini (TIP) and Yanamono (YAM).

HESSD
10, 15295–15335, 2013

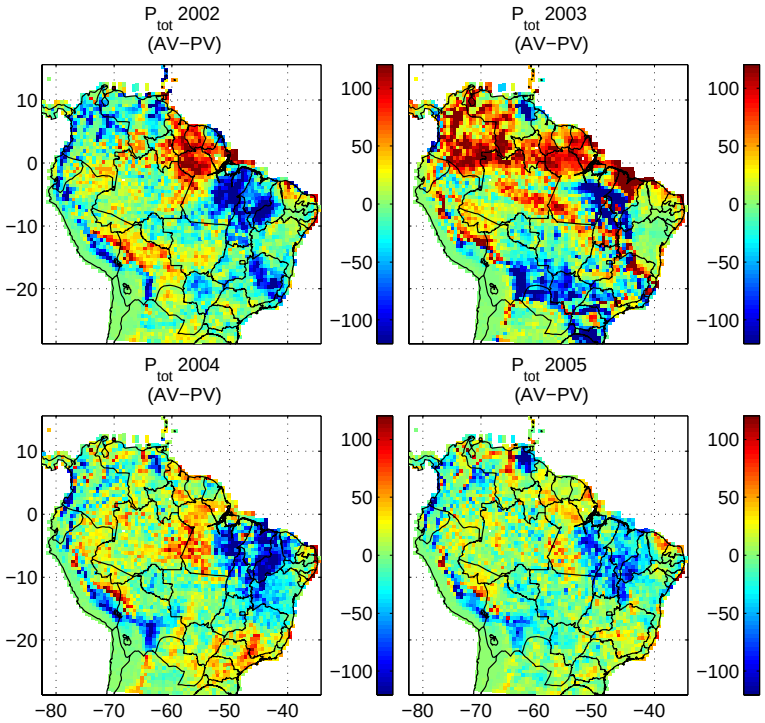

Fig. 5. Differences in total annual surface precipitation [mm], 2002–2005. Potential Vegetation Condition is subtracted from the Actual Vegetation condition.

HESSD
10, 15295–15335, 2013

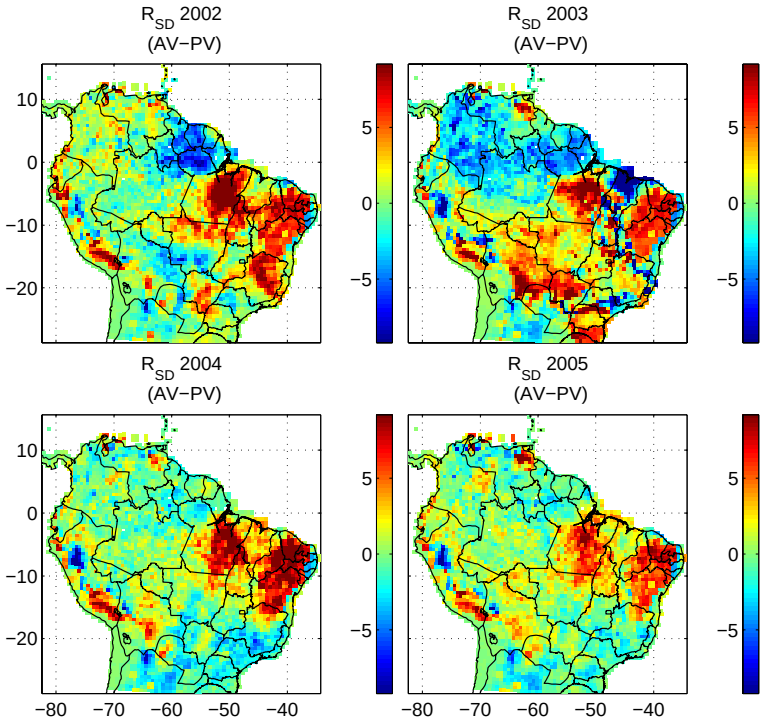

Fig. 6. Differences in mean annual down-welling surface shortwave radiation [W m^{-2}], 2002–2005. Potential Vegetation Condition is subtracted from the Actual Vegetation condition.

HESSD
10, 15295–15335, 2013

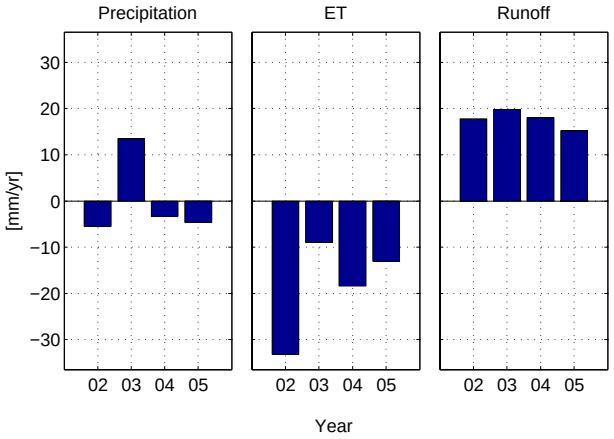

Fig. 7. Difference in mean continental precipitation, evaporation and total runoff, between the Actual Vegetation case and Potential Vegetation case (AV–PV).

HESSD
10, 15295–15335, 2013

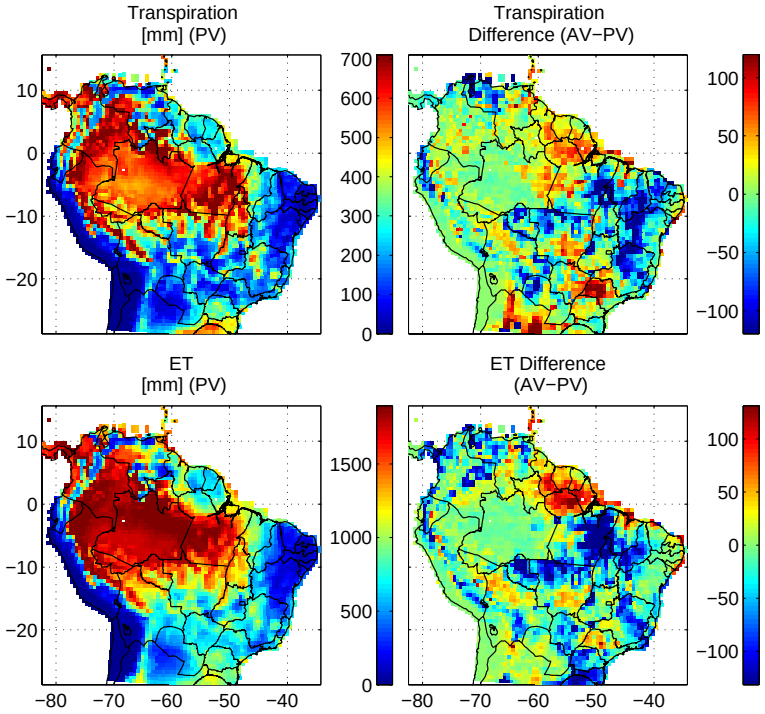

Fig. 8. Annual transpiration and evapotranspiration [mm]. Totals for the Potential Vegetation condition and differences, 2002–2005.

HESSD
10, 15295–15335, 2013

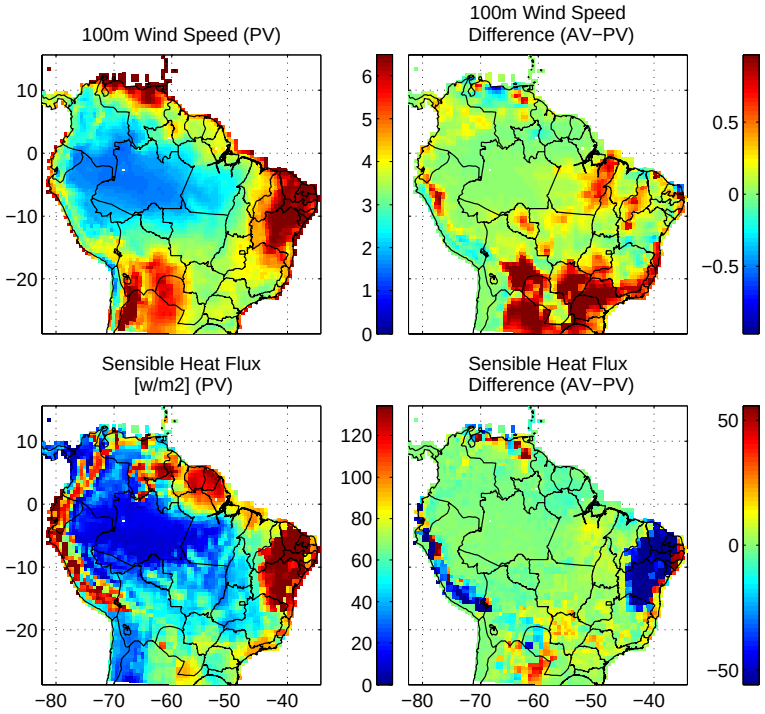

Fig. 9. Mean wind-speed [$m s^{-1}$] and sensible heat-flux [$W m^{-2}$]. Totals for the Potential Vegetation condition and differences, 2002–2005.

HESSD
10, 15295–15335, 2013

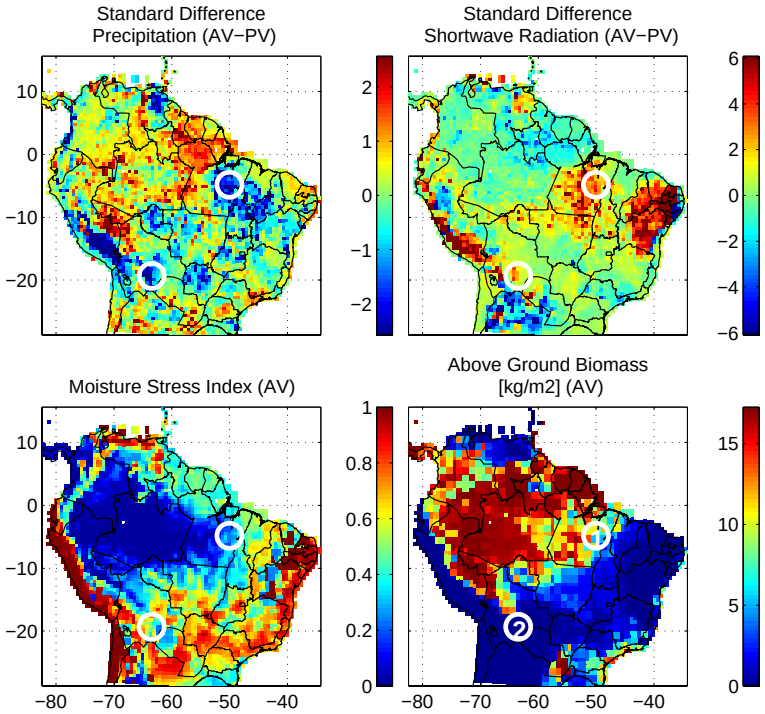

Fig. 10. Combined assessment of the regional significance in differences between precipitation and radiation, and the susceptibility of the ecosystems. Upper panels show standard scores reflecting surface precipitation and surface down-welling shortwave radiation. The lower left panel shows the moisture stress index for the (AV) scenario (see Eq. 3). For reference, (AV) scenario Above Ground Biomass is provide in the bottom right panel.

HESSD
10, 15295–15335, 2013

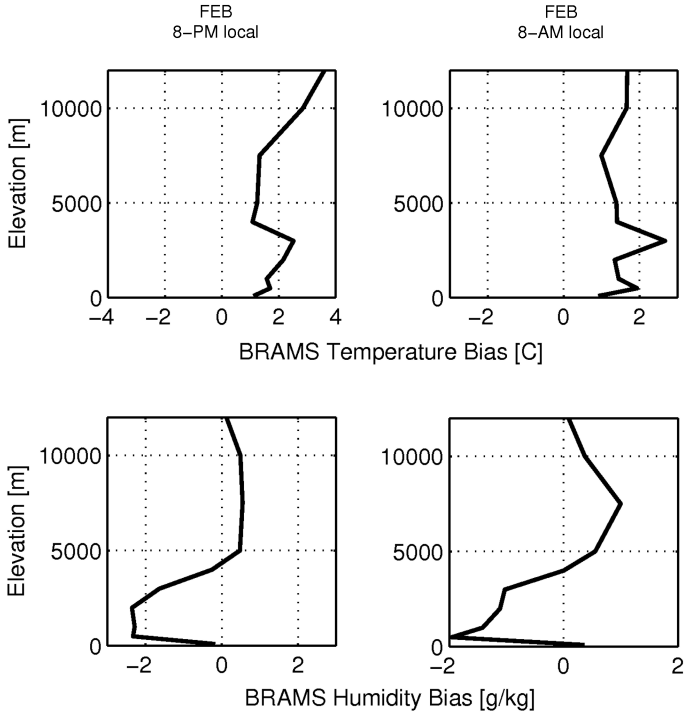

Fig. 11. Comparison of model estimates with radiosonde data, differences in mean air temperature and specific humidity. Manaus, February 2003.

HESSD
10, 15295–15335, 2013

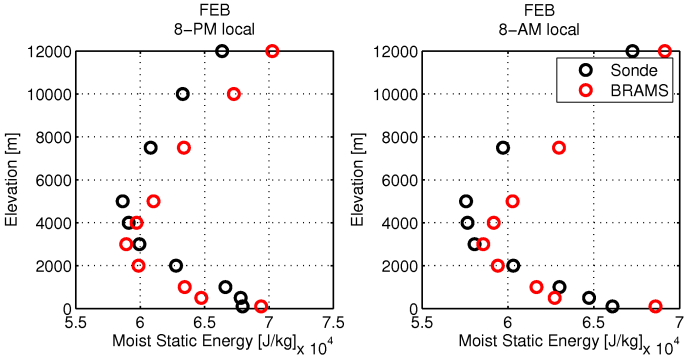

Fig. 12. Comparison of model estimates with radiosonde data, mean wind magnitude and mean moist static energy. Manaus, February 2003.

HESSD
10, 15295–15335, 2013

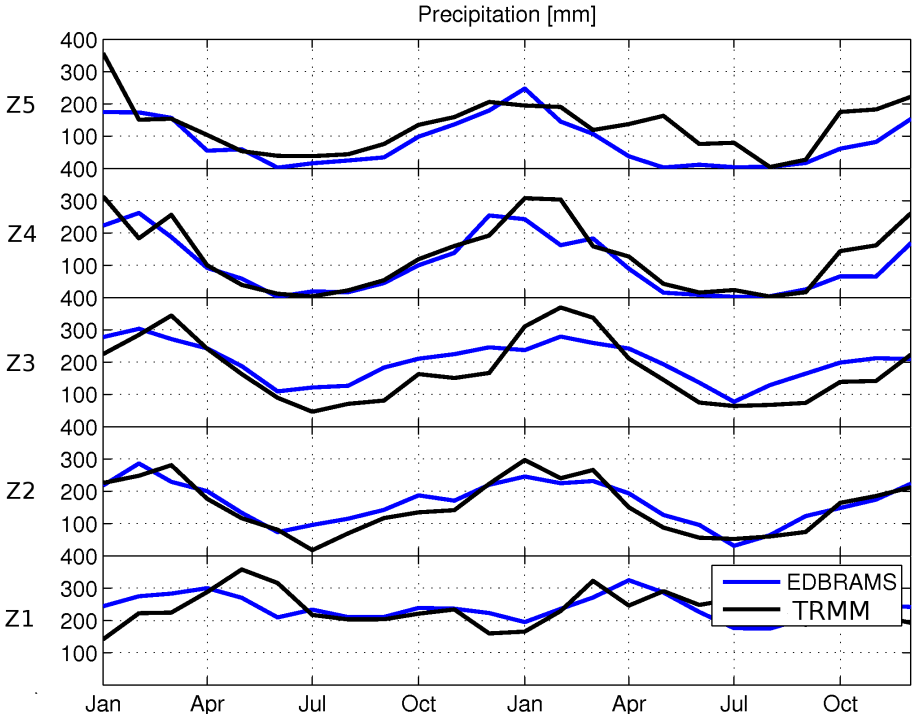

Fig. 13. Mean monthly precipitation from ED-BRAMS and the TRMM 3B43 product, years 2000–2001. Spatial means are taken within zones according to Fig. 4.

HESSD
10, 15295–15335, 2013

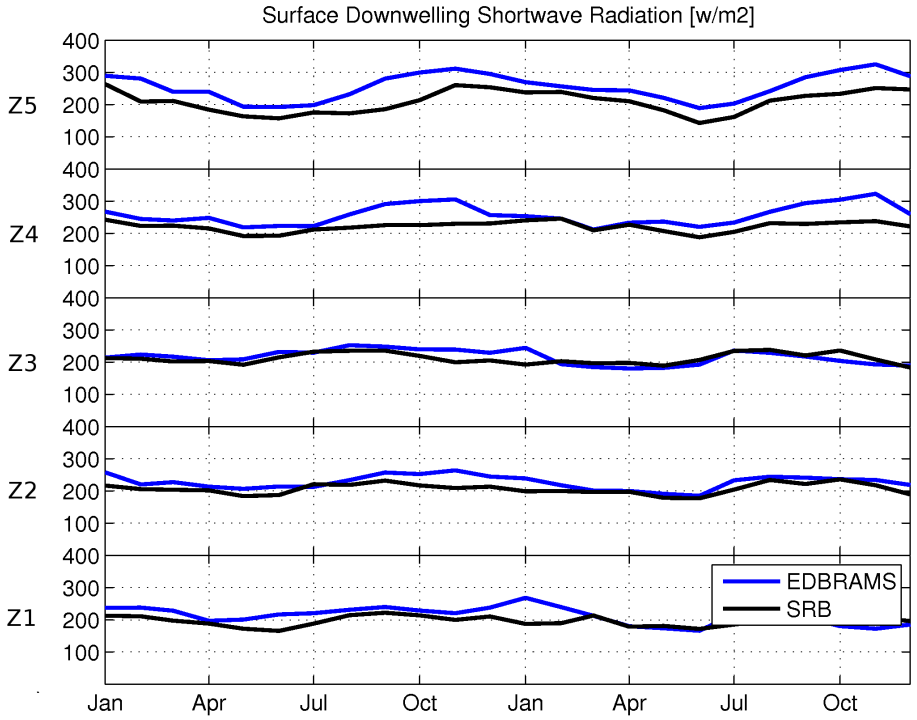

Fig. 14. Mean monthly surface radiation from ED-BRAMS and the SRB product, years 2000–2001. Spatial means are taken within zones according to Fig. 4.

HESSD
10, 15295–15335, 2013

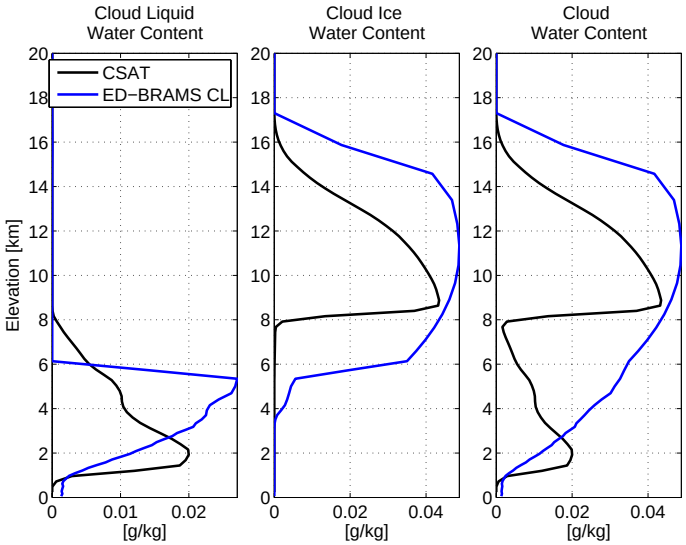

Fig. 15. CloudSat climatological water content profiles and model estimated water content profiles for February 2003, 17:00 UTC, 3° N–12° S and 70–55° W.

HESSD
10, 15295–15335, 2013